

# Design of microstrip-line coupled kinetic inductance detectors for near infrared astronomy

Shiling Yu<sup>ab</sup>, Shibo Shu<sup>c\*</sup>, Ran Duan<sup>a†</sup>, Lihui Yang<sup>d</sup>, and Di Li<sup>a</sup>

<sup>a</sup>National Astronomical Observatories, Chinese Academy of Sciences, Beijing 100101, China

<sup>b</sup>School of Astronomy and Space Science, University of Chinese Academy of Sciences, Beijing 100049, China

<sup>c</sup>Institute of High Energy Physics, Chinese Academy of Sciences, Beijing 100049, China

<sup>d</sup>Zhejiang Lab, Hangzhou, Zhejiang 311121, China

\*shusb@ihep.ac.cn

†Send correspondence to duanran@nao.cas.cn

## ABSTRACT

Kinetic inductance detectors (KID) have great potential in astronomical observation, such as searching for exoplanets, because of their low noise, fast response and photon counting characteristics. In this paper, we present the design process and simulation results of a microstrip line coupled KIDs array for near-infrared astronomical observation. Compared with coplanar waveguide (CPW) feedlines, microstrip feedlines do not require air bridges, which simplify fabrication process. In the design part, we mainly focus on the impedance transforming networks, the KID structure, and the frequency crosstalk simulations. The test array has a total of 104 resonators with 8 rows and 13 columns, which ranges from 4.899 GHz to 6.194 GHz. The pitch size is about 200  $\mu\text{m}$  and the frequency crosstalk is less than 50 kHz in simulation.

**Keywords:** Kinetic Inductance Detectors, Superconducting Resonators, Microstrip Line, Near Infrared Detectors

## 1. INTRODUCTION

In the "Pathways to Discovery in Astronomy and Astrophysics for the 2020s", the main scientific research topics can be summarized in three directions: exploring the livable world, the dynamic universe, and the galaxy evolution<sup>1</sup>. Among them, the search for exoplanets, the characteristics and structure of dark matter halo, and the chemical evolution of galaxies all need and rely on the improvement of infrared detector technology. For example, direct imaging will provide the profile of the exoplanet atmosphere, and may also provide the present evidence of gases that could indicate life<sup>2</sup>. So far a total of 5035 exoplanets have been found, but only 59 have been found by direct imaging<sup>2</sup>.

Kinetic inductance detector emerges as the times require. For the high contrast direct imaging of exoplanets, KID will actively suppress speckles because of its high near-infrared sensitivity, lack of reading noise and fast reading characteristics<sup>3</sup>. In addition, KID can count photons and has the intrinsic spectral resolution. At present, the astronomical instruments using KID in the near-infrared band include ARCONS<sup>4</sup>, DARKNESS<sup>5</sup>, and MEC<sup>6,7</sup>. All these instruments use CPW feedlines to realize intrinsic frequency domain multiplexing readout<sup>4,5,7</sup>. The fabrication of CPW coupled KID arrays requires air bridges to suppress other CPW modes<sup>8</sup>. Using microstrip feedlines can simplify the fabrication process. Therefore, we demonstrate the design and simulation results of a microstrip-line coupled KIDs test array for near-infrared detection.

### 1.1 Basic principle of KID

When the photon energy absorbed by the superconducting material is higher than the gap energy, Cooper pairs will be broken, which changes the inductance impedance and shifts the resonance frequency to lower frequency. The change of the resonance frequency depends on the number of Cooper pairs destroyed by the incident photons, so it is directly proportional to the energy deposited in the superconductor. By reading out the change values of resonators, the photon position, arrival time, number and energy information can be obtained<sup>3,9</sup>.

The gap energy is calculated as  $2\Delta = 3.52k_B T_c$ , where  $k_B$  is the Boltzmann constant,  $T_c$  is the transition temperature, and  $\Delta$  is the gap energy. Taking aluminum film as an example,  $T_c$  is 1.18 K, and  $2\Delta$  is about  $3.582 \times 10^{-4}$  eV. Therefore, photons can be detected as long as their wavelength is shorter than 3.46 mm. Near infrared photons with wavelength range of 780 nm - 3000 nm is 0.41 eV - 1.59 eV, much larger than the gap energy of usual superconductors.

## 2. DESIGN AND SIMULATION

The most critical structure in the design of a KIDs array is the superconducting resonator. The effect of resonator pixel size, pitch size and arrangement on frequency crosstalk can be simulated by Sonnet<sup>10</sup>.

The design parameters are set as a 18 nm upper aluminum film with  $L_s = 2$  pH/sq, a 150  $\mu\text{m}$ -thick high resistance silicon with a dielectric constant of 11.7, and a 200 nm aluminum film as ground. In the future, we will switch to low reflectivity superconducting materials. The simulation setup detail are shown in Appendix A and Appendix B. The design includes four main parts, the impedance transforming networks, the KIDs, the frequency crosstalk simulation, and the pitch and arrangement.

### 2.1 Impedance transforming networks

The width of the microstrip determines the characteristic impedance of the feedline. To make the pixels compact, the microstrip width is decreased to 6  $\mu\text{m}$ , and the corresponding characteristic impedance value is 140  $\Omega$ . To match the 50  $\Omega$  cables, an impedance transformation network is used<sup>11</sup> and the calculation process is shown in Appendix C. The network design has 10 sections, which have the same length but different impedance, shown in Fig. 1. The simulation result in Fig. 2 shows that  $S_{11}$  is less than -10 dB in the range of 4 GHz - 8 GHz.

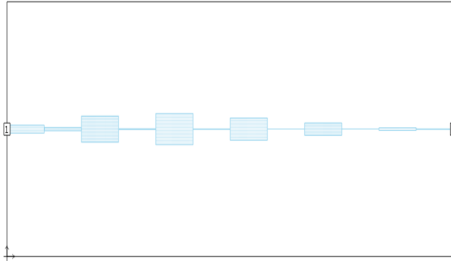


Figure 1. Impedance transforming networks

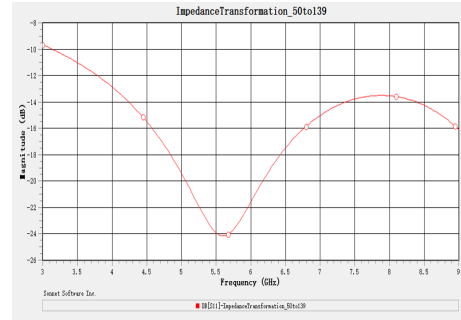


Figure 2. Simulation results  $S_{11}$

### 2.2 Superconducting resonators

The resonators are coupled capacitively to the microstrip line. The design of a lumped-element resonator is composed of a meandered inductor and an interdigitated capacitor<sup>12</sup>, both of them with 1  $\mu\text{m}$  linewidth and 0.5  $\mu\text{m}$  spacing, as shown in Fig. 3. In addition, a rectangular frame is added to reduce the frequency crosstalk<sup>13</sup>. The inductor is the main sensitive part of the photon event, with the size of 50.5  $\mu\text{m} \times 50.5 \mu\text{m}$ . The interdigitated capacitor contains 19 pairs of fingers to adjust different resonant frequencies, with the size of 126  $\mu\text{m} \times 61.5 \mu\text{m}$ . The finger length varies from 64  $\mu\text{m}$  to 121  $\mu\text{m}$ , and the adjustable frequency range is about from 4 GHz to 10 GHz. The overall size is 130  $\mu\text{m} \times 116 \mu\text{m}$ , as shown in Fig. 4.

The detail parameters are optimized to make the resonator have the appropriate quality factor. The quality factor is defined as the resonant frequency multiplied by the ratio of the average stored energy to the energy loss. The relationship among the total quality factor  $Q$ , the coupling quality factor  $Q_c$  and the internal quality factor  $Q_i$  is as follows:

$$\frac{1}{Q} = \frac{1}{Q_i} + \frac{1}{Q_c} \quad (1)$$

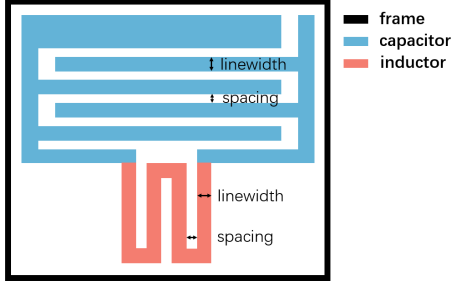


Figure 3. Design Diagram

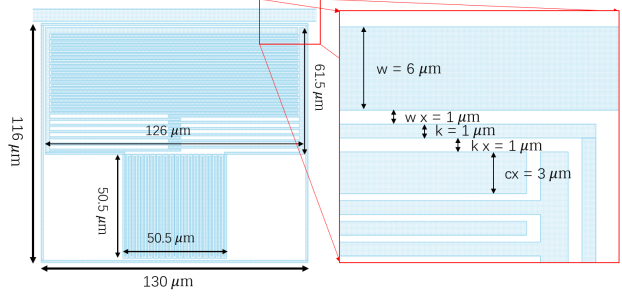


Figure 4. Description of Resonator Size

$Q_c$  represents the coupling between the resonator and the feedline. By testing the effect of the five variables shown in Fig. 4 on the quality factor  $Q_c$ , the design values are determined as ( $\mu\text{m}$ ):  $w = 6$ ,  $wx = 1$ ,  $k = 1$ ,  $kx = 1$ ,  $cx = 3$ . The resonance frequency is between 4.899 GHz and 6.194 GHz, and the corresponding quality factor  $Q_c$  is between 51.0 k and 25.3 k.

### 2.3 Frequency crosstalk simulation

In order to reduce the interaction between pixels, it is necessary to simulate the frequency crosstalk between resonators. Here, we consider three configurations, which have the greatest impact on the reference resonator, the horizontal direction, the vertical direction and the resonators placed on two sides of the feedline<sup>13</sup>. The frequency crosstalk is defined as the frequency shifts between the resonance frequencies simulated in a single resonator setup and a two-resonator setup.

#### 2.3.1 Crosstalk between resonators in the horizontal direction

In Fig. 5, two resonators with frequency difference of 8 MHz are placed at a horizontal distance of  $200 \mu\text{m}$ . Fig. 6 shows that when  $X$  is larger than  $200 \mu\text{m}$ , the crosstalk is almost constant and less than 40 kHz.

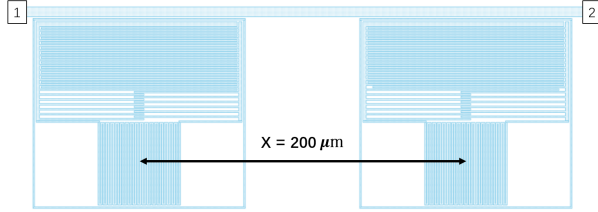


Figure 5. Simulation setup in horizontal direction

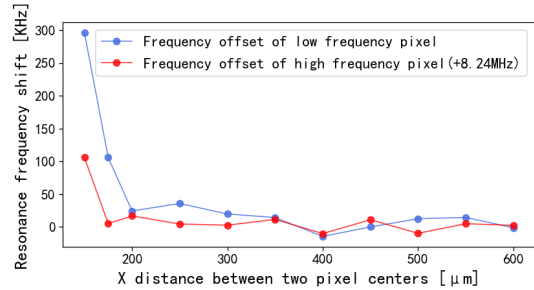


Figure 6. The crosstalk with different X distance

#### 2.3.2 Crosstalk between resonators in the vertical direction

In Fig. 7, two resonators with frequency difference of 530 MHz are placed at a vertical distance of  $363 \mu\text{m}$  (the distance between inductance parts is  $185.5 \mu\text{m}$ ). Fig. 8 shows the simulated crosstalk by varying  $2Y$ . When  $2Y > 350 \mu\text{m}$ , the crosstalk is almost constant around 35 kHz. The maximum value of  $S_{41}$  curve obtained by simulation shows the maximum crosstalk between the two feedlines, which is smaller than -22 dB when  $2Y > 350 \mu\text{m}$ .

#### 2.3.3 Crosstalk between resonators on two sides of the feedline

In Fig. 9, two resonators with different resonance frequencies are placed on two sides of the feedline, and the distance between the inductance parts is  $185.5 \mu\text{m}$ . Here we consider the crosstalk between resonators on two sides of the feedline by varying the resonance frequency difference between these two resonators. Fig. 10 shows that the crosstalk is almost constant, around 40 kHz, when the frequency difference is larger than 27.6 MHz.

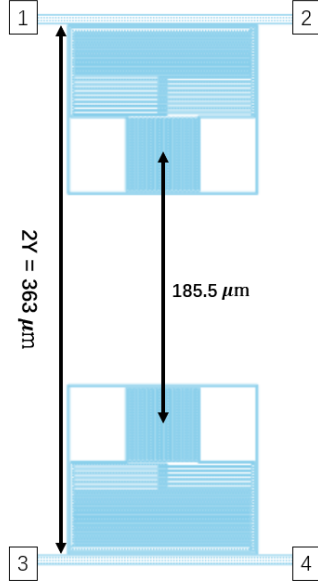


Figure 7. Simulation setup in the vertical direction

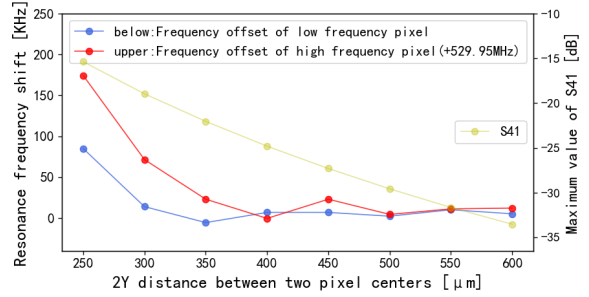


Figure 8. The simulated crosstalk by varying  $2Y$ .

The fluctuation of the simulated crosstalk may come from the numerical error when the cell size is much smaller than the wavelength in Sonnet.

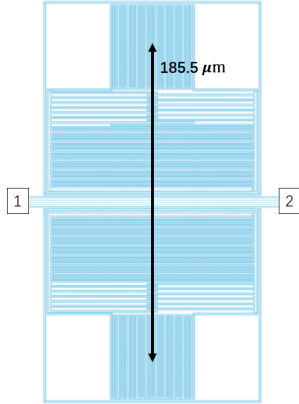


Figure 9. Simulation setup on two sides of the feedline

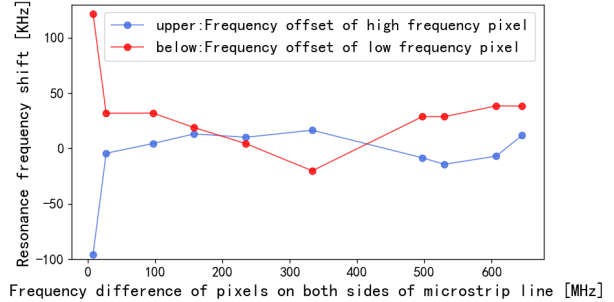


Figure 10. The crosstalk with different resonance frequency

## 2.4 Pitch size and pixel arrangement

A test array with 104 pixels is designed for testing. To minimize the crosstalk, the horizontal pitch size  $X$  is set to be  $200 \mu\text{m}$ . To have a uniform pitch size in the vertical direction,  $2Y$  is set to be  $363 \mu\text{m}$  and the vertical pitch size is  $185.5 \mu\text{m}$ . To have  $Q_c$  around 30 k, the resonance frequency range of  $4.899 \text{ GHz} - 6.194 \text{ GHz}$  is used, with a resonance frequency spacing of  $12.57 \text{ MHz}$ . The frequency difference between the resonators on two sides of the feedline is set to be  $654 \text{ MHz}$ , the half readout frequency range in our test array. The capacitor finger lengths are interpolated from the results in Fig. 11. The final test array has 104 pixels in 8 rows and 13 columns, as shown in Fig. 12.

## 3. CONCLUSION

We present a microstrip line coupled KID array design for near-infrared astronomy. An impedance transformation network is used to match the  $140 \Omega$  feedline impedance to the  $50 \Omega$  cable. The size of a single resonator is  $130$

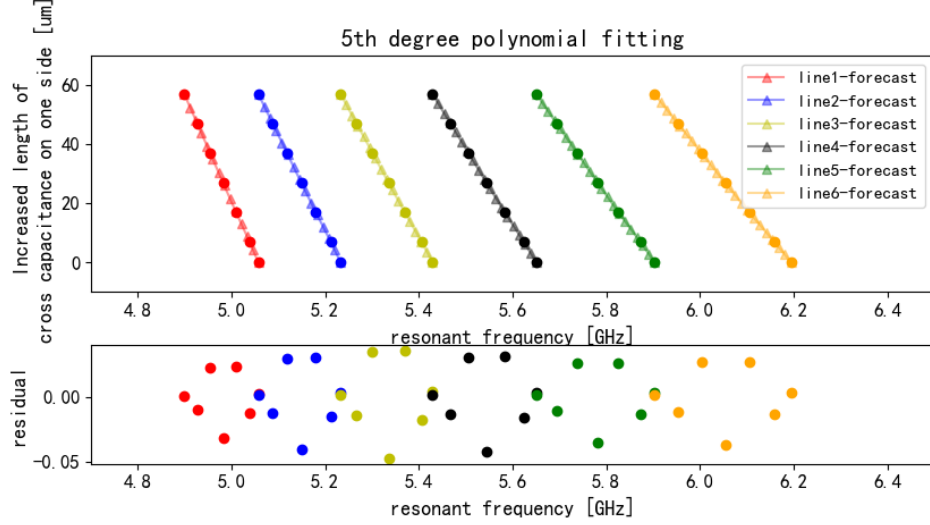


Figure 11. Polynomial fitting results between the length of capacitor fingers and the resonance frequency<sup>14</sup>.

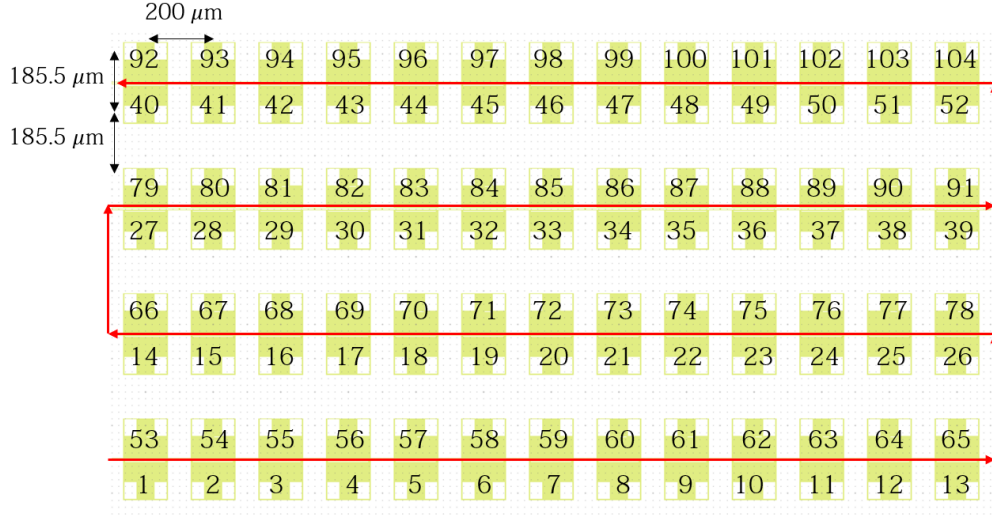


Figure 12. The pitch sizes and pixel arrangement of 104 pixels. The index shows the frequency numbering from 4.899 GHz to 6.194 GHz.

$\mu\text{m} \times 116 \mu\text{m}$ , with a square inductor of  $50.5 \mu\text{m} \times 50.5 \mu\text{m}$ . The horizontal and vertical pitch sizes are set to be  $200 \mu\text{m}$  and  $185.5 \mu\text{m}$ , respectively. The frequency crosstalks are simulated in three configurations, and the simulation results are less than 50 kHz. A test array of 104 resonators in 8 rows and 13 columns ranges from 4.899 GHz to 6.194 GHz with the frequency interval of 12.57 MHz, and the  $Q_c$  value range is 25.3 k - 51.0 k. And the measurement of photon response and noise equivalent power is in progress.

## APPENDIX A. PREPARATION

Due to the limitation of fabrication, aluminum thin film is selected as the superconducting material. Considering the high reflectivity of aluminum, other superconducting materials with high absorptivity will be used in the future.

The microstrip transmission line is composed of a  $w$  width conductive strip on the surface of a dielectric plate with a thickness of  $h$ , and a layer of conductive grounding is under the dielectric plate<sup>12</sup>. The fabrication

parameters are designed as: 18 nm upper aluminum film with  $L_s = 2$  pH/sq; 150  $\mu\text{m}$  ( $h = 150$   $\mu\text{m}$ ) high resistance silicon dielectric with a dielectric constant of 11.7; 200 nm bottom aluminum film grounding.

Before the formal design simulation, the appropriate basic unit size needs to be set. Too large cell size will lead to inaccurate simulation results, and too small cell size will take more time. Therefore, it is necessary to test the required memory and simulation results of different cell sizes.

As shown in Tab. 1, taking the resonance frequency obtained when cell size is 0.05  $\mu\text{m}$  as the reference value, two resonators with different resonant frequencies ( about 4GHz and 8GHz ) were tested. Considering the time cost and accuracy, the cell size is finally set to 0.1  $\mu\text{m}$  and the mesh of Sonnet choose "Fine/Edge Meshing".

Table 1. The test results with different basic cell sizes and different mesh of Sonnet, include the estimation of memory (determining the simulation time) and frequency differences (high-frequency resonator and low-frequency resonator are tested respectively).

cell size [ $\mu\text{m}$ ]	0.05	0.1	0.1	0.1	0.25	0.5
mesh	Fine/Edge Meshing	Fine/Edge Meshing	Coarse/Edge Meshing	Coarse/No Edge Meshing	Fine/Edge Meshing	Fine/Edge Meshing
estimated memory	11906MB	3213MB	578MB	362MB	534MB	120MB
$F_{min}$ [GHz]	3.97849	4.00111	3.99979	4.19353	4.06933	4.18769
$\Delta$ [MHz]	0	22.62	21.3	215.04	90.84	209.2
$F_{max}$ [GHz]	7.95573	7.9995	8.19636		8.15001	8.34143
$\Delta$ [MHz]	0	43.44	240.63		194.28	385.7

## APPENDIX B. MICROSTRIP FEEDLINE

A 50  $\Omega$  microstrip feedline with 130  $\mu\text{m}$  width seriously hinders the compact arrangement of a KIDs array. It is necessary to make a narrow feedline design. An impedance transformation network is needed for this high impedance feedline. From Tab. 2, the width is finally set to 6  $\mu\text{m}$ .

Table 2. The test results of feedline width and impedance, and the length of feedline is taken as 500  $\mu\text{m}$  during test.

Microstrip linewidth [ $\mu\text{m}$ ]	Characteristic impedance [ $\Omega$ ]
6	136
8	124
10	116
126	59

If the length of the feedline is too short, the impedance value will be inaccurate. When the width is 6  $\mu\text{m}$ , the impedance value changes with the different lengths of feedline, as shown in Fig. 13. Finally, 3000  $\mu\text{m}$  long feedline is selected for subsequent simulation.

## APPENDIX C. CALCULATION PROCESS OF THE IMPEDANCE TRANSFORMATION NETWORKS

The calculation process of short step impedance transformation can be divided into four steps<sup>11</sup>.

Firstly, the ratio  $r$  and the fractional bandwidth  $w$  are calculated by the following formula:

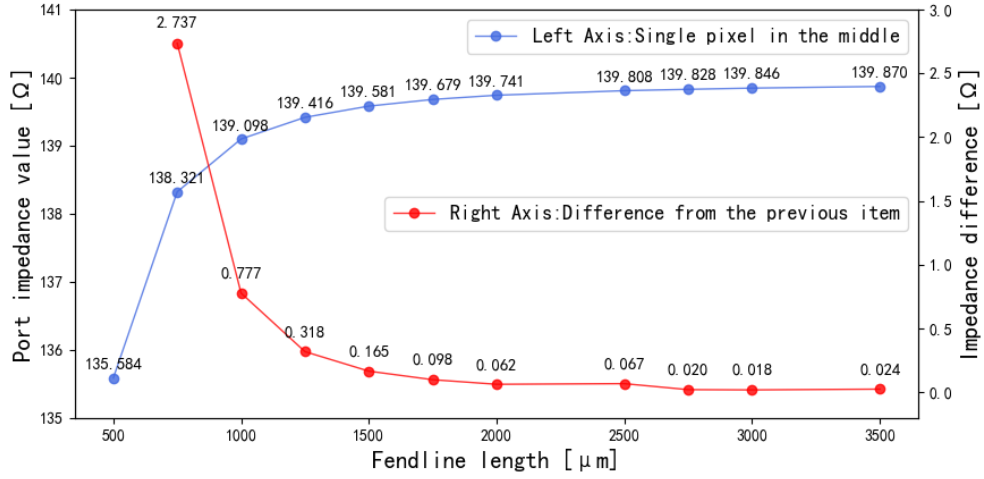


Figure 13. The impedance value gradually tends to a stable value with the increase of the length of the feedline, and the difference with the previous term tends to zero. During the test, the resonator is placed in the middle regardless of the length of the feedline.

$$r = \frac{139.846\Omega}{50\Omega} = 2.79692, w = \frac{\theta_b - \theta_a}{\frac{\theta_b + \theta_a}{2}} = \frac{(8 - 4)GHz}{\frac{(8+4)GHz}{2}} = 0.667 \quad (2)$$

Then the required  $n$  value can be determined through the table of the pass band attenuation ripple  $L_{Ar}$  in the article <sup>11</sup>, and there are:

$$n = 10, l = \frac{\lambda}{16} \quad (3)$$

Furthermore, the impedance value of half of the circuit is directly obtained from the corresponding impedance table in the article <sup>11</sup>. And the residual impedance value are calculated by equation 4.

$$Z_0 = 1 \text{ and } Z_{n+1} = r$$

$$Z_j|_{j=(n/2)+1 \text{ to } n} = \frac{r}{Z_{n+1-j}} \quad (4)$$

All normalized resistance values are then converted to actual values. The feedline widths required by the impedance value are obtained through the calculation tool. Finally, the impedance transformation network with 10 segments of the same length but different widths is drawn.

## REFERENCES

- [1] National Academies of Sciences, Engineering, and Medicine, [*Pathways to Discovery in Astronomy and Astrophysics for the 2020s*], The National Academies Press, Washington, DC (2021).
- [2] Brennan, P., "Exoplanet catalog." [EB/OL] (2022). <https://exoplanets.nasa.gov/discovery/exoplanet-catalog/> Accessed June 7, 2022.
- [3] Mazin, B., Bailey, J., Bartlett, J., Bockstiegel, C., Bumble, B., Coiffard, G., Currie, T., Daal, M., Davis, K., Dodkins, R., Fruitwala, N., Jovanovic, N., Lipartito, I., Lozi, J., Males, J., Mawet, D., Meeker, S., O'Brien, K., Rich, M., Smith, J., Steiger, S., Swimmer, N., Walter, A., Zobrist, N., and Zmuidzinas, J., "MKIDs in the 2020s," in [*Bulletin of the American Astronomical Society*], **51**, 17 (Sept. 2019).

- [4] Mazin, B. A., Meeker, S. R., Strader, M. J., Szypryt, P., Marsden, D., van Eyken, J. C., Duggan, G. E., Walter, A. B., Ulbricht, G., Johnson, M., Bumble, B., O'Brien, K., and Stoughton, C., "ARCONS: A 2024 pixel optical through near-IR cryogenic imaging spectrophotometer," *Publications of the Astronomical Society of the Pacific* **125**, 1348–1361 (nov 2013).
- [5] Meeker, S. R., Mazin, B. A., Walter, A. B., Strader, P., Fruitwala, N., Bockstiegel, C., Szypryt, P., Ulbricht, G., Coiffard, G., Bumble, B., Cancelo, G., Zmuda, T., Treptow, K., Wilcer, N., Collura, G., Dodkins, R., Lipartito, I., Zobrist, N., Bottom, M., Shelton, J. C., Mawet, D., van Eyken, J. C., Vasisht, G., and Serabyn, E., "DARKNESS: A microwave kinetic inductance detector integral field spectrograph for high-contrast astronomy," *Publications of the Astronomical Society of the Pacific* **130**, 065001 (apr 2018).
- [6] Walter, A. B., *MEC: The MKID Exoplanet Camera for High Speed Focal Plane Control at the Subaru Telescope*, PhD thesis, University of California, Santa Barbara (Jan. 2019).
- [7] Walter, A. B., Fruitwala, N., Steiger, S., Bailey, J. I., Zobrist, N., Swimmer, N., Lipartito, I., Smith, J. P., Meeker, S. R., Bockstiegel, C., Coiffard, G., Dodkins, R., Szypryt, P., Davis, K. K., Daal, M., Bumble, B., Collura, G., Guyon, O., Lozi, J., Vievard, S., Jovanovic, N., Martinache, F., Currie, T., and Mazin, B. A., "The MKID exoplanet camera for subaru SCEXAO," *Publications of the Astronomical Society of the Pacific* **132**, 125005 (nov 2020).
- [8] Szypryt, P., *Development of Microwave Kinetic Inductance Detectors for Applications in Optical to Near-IR Astronomy*, PhD thesis, University of California, Santa Barbara (Jan. 2017).
- [9] Day, P. K., LeDuc, H. G., Mazin, B. A., Vayonakis, A., and Zmuidzinas, J., "A broadband superconducting detector suitable for use in large arrays," *Nature* **425**, 817–821 (Oct. 2003).
- [10] Rautio, J. C., "Sonnet software provides commercial eda software solutions for high-frequency rf/mw electromagnetic analysis.." [EB/OL] (2022). <https://www.sonnetsoftware.com/> Accessed June 7, 2022.
- [11] Matthaei, G. L., "Short-Step Chebyshev Impedance Transformers," *IEEE Transactions on Microwave Theory and Techniques* **14**, 372–383 (Aug. 1966).
- [12] Zmuidzinas, J., "Superconducting microresonators: Physics and applications," *Annual Review of Condensed Matter Physics* **3**, 169–214 (02 2012).
- [13] Shu, S., Calvo, M., Leclercq, S., Goupy, J., Monfardini, A., and Driessen, E., "Prototype high angular resolution lekids for nika2," *Journal of Low Temperature Physics* **193** (11 2018).
- [14] Shu, S., Calvo, M., Goupy, J., Leclercq, S., Catalano, A., Bideaud, A., Monfardini, A., and Driessen, E. F. C., "Understanding and minimizing resonance frequency deviations on a 4-in. kilo-pixel kinetic inductance detector array," *Applied Physics Letters* **119**, 092601 (aug 2021).